Materials Transactions, Vol. 48, No. 7 (2007) pp. 1665 to 1670
Special Issue on Bulk Metallic Glasses —Selected Papers from the Fifth InternationalConference on Bulk Metallic Glasses (BMGV)

Nanocrystalline Transformation and Inverse Transformation in Metallic Glasses Induced by Electropulsing

H. Mizubayashi*[1], T. Takahashi*[2], K. Nakamoto*[2] and H. Tanimoto

Institute of Materials Science, University of Tsukuba, Tsukuba 305-8573, Japan

Electropulsing by means of discharge of a condenser with the decay time (τ) of ms causes the athermal crystallization of metallic glasses when the initial current density (i_{d0}) is higher than the threshold value ($i_{d0,c}$). It is indicated that the major local amorphous structures in $Zr_{50}Cu_{50}$ are the amorphous structures with the short range order (SRO) similar to crystalline cubic (*c*) ZrCu which is the equilibrium crystalline phase above 988 K, although the mixture of crystalline Zr_2Cu and Zr_7Cu_{10} is the equilibrium phase below 988 K. Electropulsing tests on $Zr_{50}Cu_{50}$, $Zr_{50}Cu_{40}Al_{10}$ and $Zr_{50}Cu_{35}Al_{10}Ni_5$ metallic glasses indicate that the amorphous structures with SRO similar to *c*ZrCu are the major local amorphous structures in these metallic glasses, and their volume fractions decrease in the order of $Zr_{50}Cu_{50}$, $Zr_{50}Cu_{40}Al_{10}$ and $Zr_{50}Cu_{35}Al_{10}Ni_5$. The amount of the amorphous structures with SRO similar to *c*ZrCu may govern the thermal stability of these metallic glasses. Further in $Zr_{50}Cu_{50}$ metallic glasses, the inverse transformation from the electropulsing-induced fine crystallites to the amorphous phase for subsequent electropulsing with increasing i_{d0}, and the Ostwald-ripening-like phenomenon under electropulsing were observed.
[doi:10.2320/matertrans.MJ200726]

(Received November 14, 2006; Accepted February 13, 2007; Published June 20, 2007)

Keywords: *metallic glass, phase transformation, crystallization, collective motion, electromigration*

1. Introduction

After finding of acceleration of the thermal crystallization in metallic glasses by an electric direct-current of 10^7 A/m^2,[1] or repetition of electric square pulses of 10^9 A/m^2 with about 0.1 ms duration for one hour, a total of a few seconds for passing current,[2] many works have been done to getting insight into the underlying mechanism. Under passing of an electric direct-current of 10^7 A/m^2, a decrease in the crystallization temperature, T_x, by 10 to 20 K due to the enhancement of the homogeneous nucleation process was found in $Ti_{50}Cu_{50}$, $Zr_{50}Cu_{50}$ and $(Zr_{70}Cu_{30})_{92.5}Al_{7.5}$ metallic glasses.[3–6] Under the repetition of electric square pulses of 10^9 A/m^2, a decrease in T_x by 150 to 170 K was observed in Fe-Si-B metallic glasses, where enhancement of atomic diffusion by the stochastic resonance was claimed to take place.[7–9] It is known that both passing of an electric direct-current of 10^7 A/m^2 and the repetition of electric square pulses of 10^9 A/m^2 with a total of a few seconds for passing current cause no detectable changes in crystalline Al and Cu circuits.[10] In order to explain the observed effects of passing electric current, the concentration of electromigration force associated with a collective motion of many atoms should be taken into account.

Besides the effects of passing electric current, a considerable decrease in the dynamic Young's modulus in the frequency range between 10^2 and 10^4 Hz has been commonly observed for $Pd_{80}Si_{20}$, $Ti_{50}Cu_{50}$, $Zr_{50}Cu_{50}$ and $Zr_{60}Cu_{30}Al_{10}$ metallic glasses, suggesting that a resonant collective motion of many atoms can be excited by elastic vibrations at a strain amplitude of 10^{-6}.[11,12] The combination of the effects of passing electric current and the decrease in the dynamic Young's modulus predicts that a resonant collective motion of many atoms may be excited by resonant-electropulsing too. Such electropulsing can be made by discharge of a condenser. During electropulsing, the current density, i_d, decays with increasing elapsed time, t, as,

$$i_d = i_{d0} \exp(-t/\tau), \tag{1}$$

where i_{d0} is the initial value of i_d and τ is the decay time of discharge. It is known that the frequency of the principal Fourier constituent of (1) is $1/2\pi\tau$, i.e., $1/2\pi\tau$ may be tuned to excite a resonant collective motion by adjusting τ.

Experimentally, it has been found that a single electropulsing with τ of about 1 ms causes the crystallization of $Pd_{80}Si_{20}$, $Ti_{50}Cu_{50}$, and $Zr_{60}Cu_{30}Al_{10}$ metallic glasses below 400 K by a considerable volume fraction when i_{d0} is higher than the threshold value of 10^9 A/m^2 (the electropulsing-induced low-temperature crystallization, *e*-LTC, hereafter).[13,14] Recently, the temperature range for electropulsing tests has been extended to the liquid nitrogen (LN_2) temperature.[15] The features of the *e*-LTC observed for electropulsing tests in a LN_2 bath have been almost the same to those observed electropulsing tests near room temperature (RT), indicating that the density fluctuation responsible for the *e*-LTC is frozen at the glass transition temperature. The transmission electron microscopy observation has revealed that crystallites formed by the *e*-LTC showed crystallographic alignment with each other. Such crystallographic alignment cannot be expected when enhancement of atomic diffusion by the stochastic resonance is the underlying mechanism for the *e*-LTC. Then, it is suggested that a resonant collective motion of many atoms excited by electropulsing causes the transformation of the amorphous phase to the crystalline phase.[15] That is, a local region with an amorphous structure favorable to a crystalline structure may transform to the crystalline structure through a collective motion excited by electropulsing. In $Ti_{50}Cu_{50}$, crystalline TiCu was commonly formed in the *e*-LTC by electropulsing and the thermal crystallization at elevated temperatures, where a decrease in the specimen resistivity due to single electropulsing was as large as one half of that observed after the thermal crystallization.[15] These observed results indicate

*[1]Corresponding author. E-mail: mizuh@ims.tsukuba.ac.jp
*[2]Graduate Student: University of Tsukuba

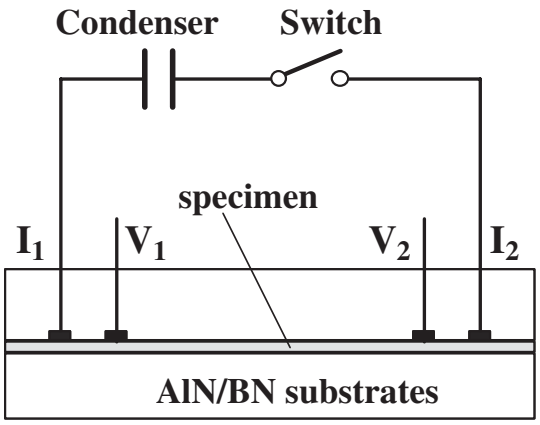

Fig. 1 The measurement setup for electropulsing.

that the local amorphous structures in $Ti_{50}Cu_{50}$ metallic glass are favorable to that of crystalline TiCu. Then, the *e*-LTC by electropulsing in $Zr_{50}Cu_{50}$ metallic glass is expected to induce the formation of cubic (*c*) ZrCu which is the high temperature crystalline phase above 988 K,[16] although crystalline Zr_7Cu_{10} and Zr_2Cu are formed in the thermal crystallization at elevated temperatures.

In the present work, this prediction was pursued in $Zr_{50}Cu_{50}$ metallic glass, where the predicted phenomenon was observed. Furthermore, the inverse transformation from the crystalline phase to the amorphous phase was observed too. These observed results will be given below together with the preliminary data observed in $Zr_{50}Cu_{40}Al_{10}$ and $Zr_{50}Cu_{35}Al_{10}Ni_5$ metallic glasses.

2. Experiment

Thin tapes of $Zr_{50}Cu_{50}$, $Zr_{50}Cu_{40}Al_{10}$ and $Zr_{50}Cu_{35}Al_{10}Ni_5$ metallic glasses were prepared by melt spinning in a high-purity Ar gas atmosphere. Both surfaces of a tape specimen were smoothed by polishing mechanically using fine emery paper in water avoiding heat-up during polishing. The thickness and width of specimens after polishing were about 20 μm and 0.9 mm. Figure 1 shows the measurement setup for electropulsing which was similar to that reported in the previous works.[13–15] A specimen was sandwiched by two aluminum nitride (AlN)/boron nitride (BN)-composite substrates with the thermal conductivity of $90\,W{\cdot}K^{-1}{\cdot}m^{-1}$ to minimize an effect of joule heating during electropulsing. The electric resistivity of a specimen, *R*, was measured before and after each electropulsing to monitor the *e*-LTC. Electropulsing experiments were carried out at RT and in a LN_2 bath. The X-ray diffraction (XRD) measurements were made by the θ-2θ scan using the Cu-K_α radiation, where reflections from Si powder put on a specimen surface were used as reference. The microstructure of a specimen was investigated by the TEM.

3. Results

Figure 2(a) shows an example of resistivity changes in a $Zr_{50}Cu_{50}$ specimen observed after electropulsing with $\tau \sim 4.3$ ms at RT. In Fig. 2(a), the normalized resistivity, R/R_0, is plotted against i_{d0} (the bottom horizontal axis) and also against P_d (the upper horizontal axis), where R_0 denotes the resistivity of a virgin specimen and P_d is the electric energy of single electropulsing given to the unit volume of a specimen. It is noted that each data point was observed after single electropulsing. The *e*-LTC started when i_{d0} increased beyond the threshold value, $i_{d0,c}$, which was 1.4×10^9 A/m^2 and corresponded to P_d of 7.9 J/mm^3 in Fig. 2(a). Figure 2(b) shows examples of the specimen temperature, *T*, *vs.* elapsed time, *t*, data observed for electropulsing with $\tau \sim 4.3$ ms. The specimen temperature increased to its maximum temperature, T_{max}, in 10 milliseconds and then decreased in a few tens of milliseconds. In Figure 2(c), the maximum increase in the specimen temperatures, ΔT_{max}, observed for three specimens during electropulsing with $\tau \sim 4$ ms are shown, where ΔT_{max} increased linearly with P_d. Figure 3 shows the time-temperature-transformation (TTT) diagram for $Zr_{50}Cu_{50}$, where the data reported for the thermal crystallization[17–21] are shown too. The *T vs. t* data 2 shown in Fig. 2(b) is redrawn on the TTT diagram which indicates that no thermal crystallization is expected during electropulsing.

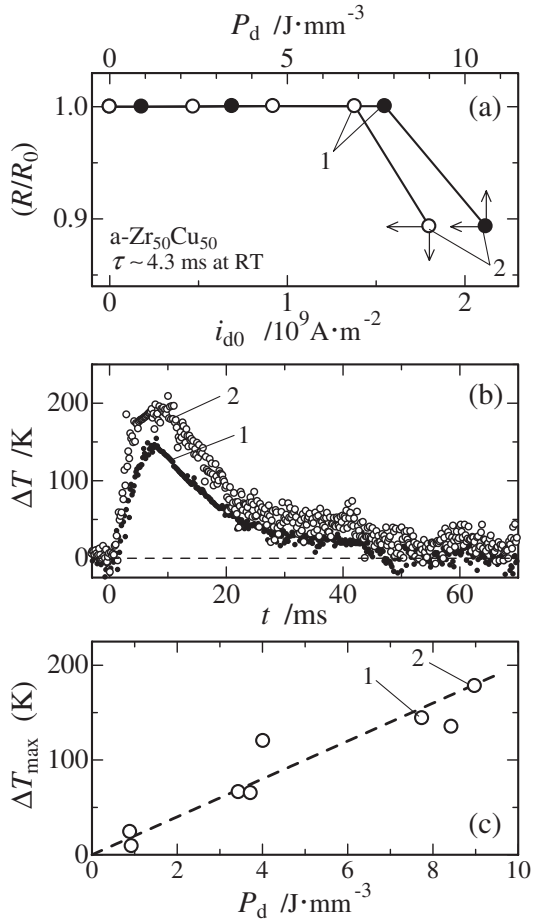

Fig. 2 (a) Changes in *R* at RT observed for a $Zr_{50}Cu_{50}$ specimen after electropulsing with $\tau = 4.3$ ms near RT, where the observed data are plotted against i_{d0} (the open symbols) and against P_d (the filled symbols) too. (b) Changes in *T* observed during electropulsing for the data points 1 and 2 in (a). (c) The ΔT_{max} *vs.* P_d data observed during electropulsing with $\tau \sim 4$ ms for various specimens. The data points 1 and 2 denote ΔT_{max} found in (b). The dashed line is drawn to guide eyes.

Figure 4(a) shows examples of resistivity changes in

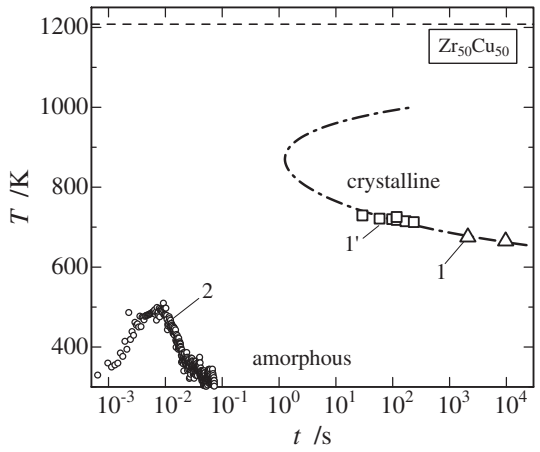

Fig. 3 The TTT-diagram for $Zr_{50}Cu_{50}$. The open triangles-1[17] denote the incubation time t_x for the crystallization found in isothermal annealing and the open squares-1'[18–21] denote the deduced t_x estimated from the crystallization temperature T_x found in the constant heating rate (γ) measurements by assuming the relationship $t_x = 20\,\mathrm{K}/\gamma$. The open circles -2 are the redrawing of those in Fig. 2(b). The horizontal dashed line denotes T_m.

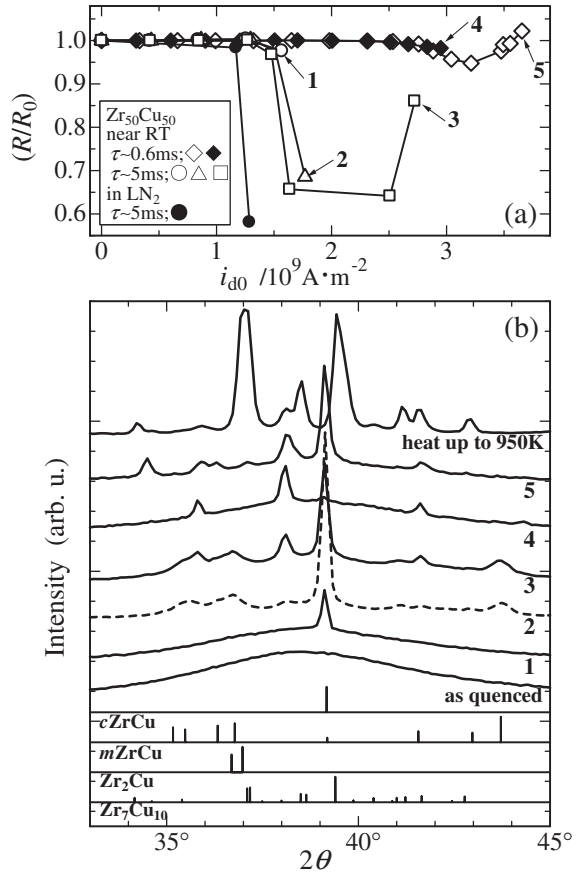

Fig. 4 (a) Changes in R at RT after electropulsing with $\tau \sim 0.6$ ms and 5 ms near RT and those in R at 78 K after electropulsing with $\tau \sim 5$ ms in LN_2 observed in $Zr_{50}Cu_{50}$ specimens. (b) XRD spectra observed after electropulsing 1 to 5 shown in (a), where XRD spectrum observed in the as quenched state and that after crystallization at 950 K are also shown. Theoretical XRD spectra for crystalline cubic-ZrCu (*c*ZrCu), monoclinic-ZrCu (*m*ZrCu), Zr_2Cu and Zr_7Cu_{10} are shown too.

$Zr_{50}Cu_{50}$ specimens observed after electropulsing with various τ at RT and that in a LN_2 bath. For electropulsing with $\tau \sim 5$ ms, R showed a strong decrease for electropulsing with i_{d0} just above $i_{d0,c}$, and then a strong increase for subsequent electropulsing with increasing i_{d0} (1 to 3 in Fig. 4(a)). The strong decrease in R after electropulsing with i_{d0} just above $i_{d0,c}$ was also observed for electropulsing in a LN_2 bath. Changes in R observed for electropulsing with shorter τ of ~0.6 ms was similar to those observed with $\tau \sim 5$ ms except that $i_{d0,c}$ increased and the magnitude of changes in R decreased, respectively. The XRD spectra observed for the specimens 1 to 5 after electropulsing are shown in Fig. 4(b) in which the XRD spectra observed for specimens in the as quenched state and after the thermal crystallization are shown too. The XRD spectrum observed after the thermal crystallization showed reflections from crystalline Zr_2Cu and Zr_7Cu_{10}. In contrast, the XRD spectrum 1 shows a reflection from *c*ZrCu. The XRD spectrum 2 shows major reflections from *c*ZrCu and monoclinic (*m*) ZrCu and minor reflections from crystalline Zr_7Cu_{10}. For the XRD spectrum 3, reflections from crystalline phases decrease and a reflection from the amorphous phase increased. The XRD spectra 4 and 5 are similar to the XRD spectrum 3.

In order to study the changes in the XRD spectra 1 to 3, the relative XRD intensity of the reflection from the amorphous phase, $I_a/(I_a + I_c)$, was evaluated as follows, where I_c is the intensity of the reflection from the crystalline phases. As already mentioned, the major reflections in the XRD spectra 1 to 3 are the reflections from *c*ZrCu and *m*ZrCu. It is not shown here but the major reflections from *c*ZrCu and *m*ZrCu can be observed for 2θ between 28 and 49 degree using the Cu-K_α radiation. In the present work, the XRD spectra as-quenched and 1 to 3 were measured for 2θ between 25 and 55 degree by step scans with 0.1 degree. The maximum number of counts per one step was, for example, 6×10^4 for the XRD spectrum as-quenched and 2×10^5 for the XRD spectrum 2, respectively. For the XRD spectrum as-quenched, the broad reflection was observed between 30 and 50 degree showing the maximum at 38.5 degree in 2θ, where I_a was evaluated as the integrated number of counts after subtraction of background values fitted by a straight line. The broad reflection found in the XRD spectrum as-quenched was applied to the XRD spectra 1 to 3 to estimate I_a in these XRD spectra and then, I_c was determined for the reflections from crystalline phases observed for 2θ between 25 and 55 degree. Figure 5 shows $I_a/(I_a + I_c)$ evaluated for the XRD spectra 1 to 3. $I_a/(I_a + I_c)$ showed the parallel change with R seen in Fig. 4(a).

Figures 6(a) and 6(b) show TEM images observed for the specimens 2 and 3 shown in Fig. 4(a). The specimen 2 showed a strong decrease in R to $0.68R_0$ after electropulsing, and *c*ZrCu crystallites with the diameter of several nm are seen in Fig. 6(a). The specimen 3 showed a strong decrease in R to $0.64R_0$ followed by an increase in R to $0.87R_0$ after subsequent electropulsing, and *c*ZrCu crystallites with the diameter of a few tens of nm are seen in Fig. 6(b), i.e., the ripening of *c*ZrCu crystallites and the increase in the volume fraction of the amorphous mentioned in Fig. 5 took place simultaneously.

Figures 7(a) shows examples of resistivity changes in

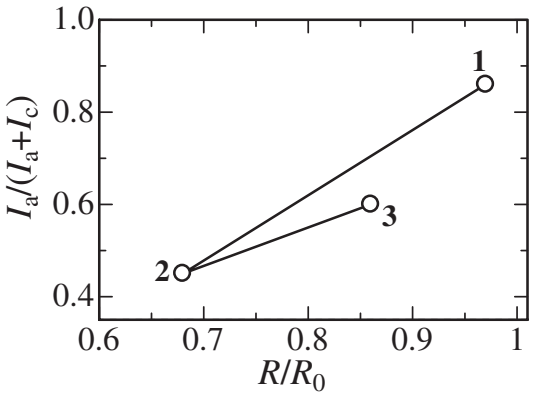

Fig. 5 The fractional XRD intensity from the amorphous phase, $I_a/(I_a + I_c)$, where I_a and I_c are the XRD intensities from the amorphous phase and the crystalline phases, respectively. The data points 1 to 3 were determined from XRD spectra observed for $Zr_{50}Cu_{50}$ after electropulsing 1 to 3 shown in Fig. 4(a), respectively.

$Zr_{50}Cu_{50}$, $Zr_{50}Cu_{40}Al_{10}$ and $Zr_{50}Cu_{35}Al_{10}Ni_5$ metallic glasses after electropulsing at RT. It is not shown here but the general features of the *e*-LTC are similar among these metallic glasses except that the magnitude of changes in R decreased in the order of $Zr_{50}Cu_{50}$, $Zr_{50}Cu_{40}Al_{10}$ and $Zr_{50}Cu_{35}Al_{10}Ni_5$ metallic glasses. Figure 7(b) shows the XRD spectra observed in the specimens shown in Fig. 7(a). The reflection from *c*ZrCu was the major reflection in all the metallic glasses.

4. Discussion

The *T vs. t* data observed during electropulsing depicted on the TTT diagram (Fig. 3) indicate that the *e*-LTC in $Zr_{50}Cu_{50}$ was due to the transformation of the amorphous phase to the crystalline phases in which the thermal diffusion beyond an atomic distance was not expected. The R *vs.* i_{d0} data (Fig. 4(a)) and the XRD spectra (Fig. 4(b)) indicate that the major local amorphous structures in $Zr_{50}Cu_{50}$ are the amorphous structures with SRO similar to *c*ZrCu, and the amounts of the crystalline phases formed by a single electropulsing are a function of τ.

As already mentioned, a resonant collective motion of many atoms can be excited by elastic vibration resulting in the decrease in the dynamic Young's modulus, E_d, from the

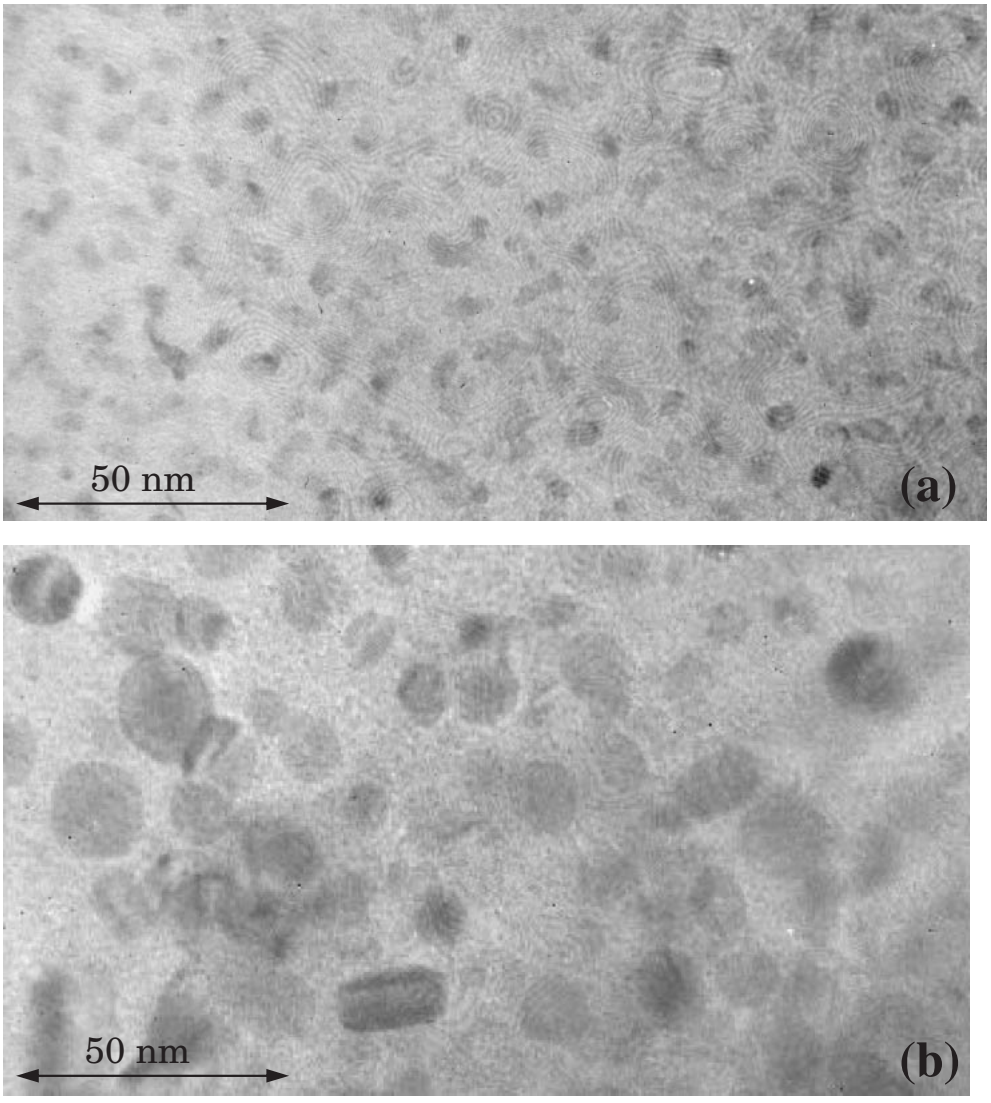

Fig. 6 TEM images (a) and (b) observed for $Zr_{50}Cu_{50}$ after electropulsing 2 and 3 shown in Fig. 4(a), respectively.

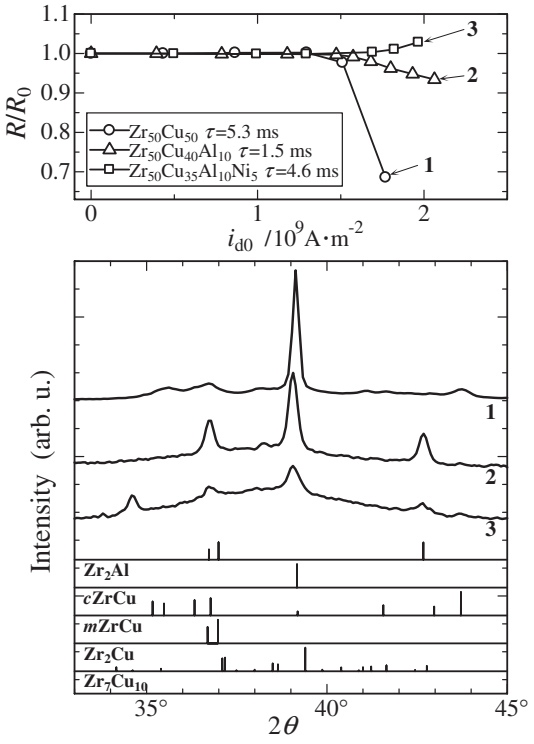

Fig. 7 (a) Examples of changes in R at RT after electropulsing at RT in $Zr_{50}Cu_{50}$ with $\tau = 5.3$ ms, $Zr_{50}Cu_{40}Al_{10}$ with $\tau = 1.5$ ms, and $Zr_{50}Cu_{35}Al_{10}Ni_5$ with $\tau = 4.6$ ms. (b) XRD spectra observed after electropulsing 1 to 3 shown in (a), where theoretical XRD spectra for crystalline Zr_2Al, *c*ZrCu, *m*ZrCu, Zr_2Cu and Zr_7Cu_{10} are shown too.

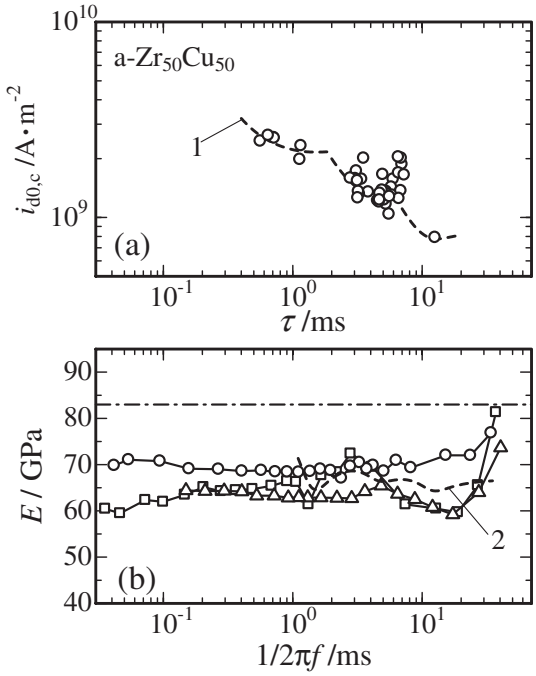

Fig. 8 (a) The $i_{d0,c}$ *vs.* τ data observed for electropulsing at RT. (b) The E_d *vs.* f data observed at RT.[21] The dot and dashed line denotes E_s. See text for curves 1 and 2.

static Young's modulus, E_s. Such resonant collective motion of many atoms may be excited by electropulsing resulting in *e*-LTC. For $Pd_{80}Si_{20}$, $Ti_{50}Cu_{50}$ and $Zr_{60}Cu_{30}Al_{10}$ metallic glasses, a close correlation between the $i_{d0,c}$ *vs.* τ data observed for the *e*-LTC and the E_d *vs.* f data observed for the dynamic elastic response has been found.[15] For $Zr_{50}Cu_{50}$ metallic glass, Figure 8(a) shows the $i_{d0,c}$ *vs.* τ data found for electropulsing at RT in the present work and Figure 8(b) is the E_d *vs.* f data which is redrawing of Fig. 2(a) in Ref. 21, respectively. The dashed curve 1 in Fig. 8(a) and the dashed curve 2 in Fig. 8(b) are fitted to the $i_{d0,c}$ *vs.* τ data and the E_d *vs.* f data, respectively, by assuming that the *e*-LTC takes place when the amplitude of resonant collective motion is increased beyond the threshold value and the decrease in E_d is associated with anelastic strains due to the resonant collective motions (see Ref. 15, for details). It is assumed for the curve 1 in Fig. 8(a) that the resonant collective motions can be excited by electropulsing with τ_r of 1.5, 5 and 13 ms. Then, the curve 2 in Fig. 8(b) is fitted to the E_d *vs.* f data by assuming the resonant collective motions at around $f_r = 1/(2\pi\tau_r)$. Although the number of data points for both the $i_{d0,c}$ *vs.* τ data and the E_d *vs.* f data is limited, a close correlation between these data may be recognized. As mentioned in Fig. 4(a), the strong *e*-LTC takes place near $\tau = 5$ ms, suggesting that resonant collective motions of the most of the amorphous structures with SRO similar to *c*ZrCu can be excited at around $f_r \sim 30\,s^{-1}$ with $\tau_r = 5$ ms.

The R *vs.* i_{d0} data (Fig. 7(a)) and the XRD spectra (Fig. 7(b)) observed in $Zr_{50}Cu_{50}$, $Zr_{50}Cu_{40}Al_{10}$ and $Zr_{50}Cu_{35}Al_{10}Ni_5$ indicate that the amorphous structures with SRO similar to *c*ZrCu are commonly the major local amorphous structures in these metallic glasses, and their volume fractions decrease in the order of $Zr_{50}Cu_{50}$, $Zr_{50}Cu_{40}Al_{10}$ and $Zr_{50}Cu_{35}Al_{10}Ni_5$. In other words, the amount of the amorphous structures with SRO similar to *c*ZrCu may govern the thermal stability of these metallic glasses.[22,23]

For the electropulsing data 1 to 3 shown in Figs. 4 and 5, the *e*-LTC (the nanocrystalline transformation) was followed by the inverse transformation with subsequent electropulsing with increasing i_{d0}. In the nanocrystalline transformation (the data 2 in Figs. 4 to 6), *c*ZrCu crystallites with the diameter of several nm (the several-nm *c*ZrCu crystallites, below) were formed and the XRD reflection from the amorphous phase $I_a/(I_a + I_c)$ decreased. In contrast, in the inverse transformation (the data 3 in Figs. 4 to 6), the number density of the several-nm *c*ZrCu crystallites showed a strong decrease, *c*ZrCu crystallites with the diameter of a few tens of nm were observed and the XRD reflection from the amorphous phase $I_a/(I_a + I_c)$ increased. The observed phenomena are similar to the Ostwald ripening. However, it is noted that the thermal diffusion is not expected during electropulsing. A theoretical work has reported that nanocrystalline precipitates in an alloy whose specific resistivity is lower than that of the matrix can be unstable due to an increase in their free energy associated with the concentration of electric current.[24] In the present electropulsing, the disappearance of the several-nm *c*ZrCu crystallites may be due to the inverse transformation associated with an increased local electric current density. However, it is again noted that the thermal diffusion is not expected during electropulsing. In order to pursue the underlying mechanism of the diffusionless-Ostwald-ripening phenomenon under electropulsing, the further work proceeds at present.

5. CONCLUSION

Resonant-electropulsing tests on $Zr_{50}Cu_{50}$, $Zr_{50}Cu_{40}Al_{10}$ and $Zr_{50}Cu_{35}Al_{10}Ni_5$ metallic glasses indicate that the amorphous structures with SRO similar to crystalline cubic (*c*) ZrCu are the major local amorphous structures in these metallic glasses, and their volume fractions decrease in the order of $Zr_{50}Cu_{50}$, $Zr_{50}Cu_{40}Al_{10}$ and $Zr_{50}Cu_{35}Al_{10}Ni_5$. The amount of the amorphous structures with SRO similar to *c*ZrCu may govern the thermal stability of these metallic glasses. Further in $Zr_{50}Cu_{50}$ metallic glasse, the inverse transformation from the electropulsing-induced fine crystallites to the amorphous phase and the Ostwald-ripening-like phenomenon under electropulsing were observed for subsequent electropulsing with increasing i_{d0}. The present work demonstrates that electropulsing tests can be a finger print test for metallic glasses.

ACKNOWLEDGEMENT

Authors are deeply indebted to Profs. K. Hono (NIMS, Japan) and K. Oshima (Inst. Mater. Sci., Univ. Tsukuba) for their supports to the TEM observations. This work is partly supported by a Grant in Aid for Scientific Research and the 21st Century Center of Excellence Program from the Ministry of Education, Culture, Sports, Science and Technology, Japan.

REFERENCES

1) H. Mizubayashi and S. Okuda: Phys. Rev. B **40** (1989) 8057–8060.
2) Z. H. Lai, H. Conrad, Y. S. Chao, S. Q. Wang and J. Sun: Scripta Metall. **23** (1989) 305–310.
3) H. Mizubayashi and R. Takemoto: Defect and Diffusion Forum **95–98** (1993) 1187–1192.
4) R. Takemoto and H. Mizubayashi: Mater. Sci. Engng. **A179/180** (1994) 275–278.
5) R. Takemoto and H. Mizubayashi: Acta Metall. Mater. **43** (1995) 1495–1504.
6) R. Takemoto, M. Nagata and H. Mizubayashi: Acta Metall. Mater. **44** (1996) 2787–2795.
7) G.-Q. Teng, Y. Chao, L. Dong, Y. Geng and Z. Lai: Jpn. J. Appl. Phys. **35** (1996) 5320–5325.
8) Z. H. Lai, H. Conrad, G. Q. Teng and Y. S. Chao: Mater. Sci. Eng. A **287** (2000) 238–247.
9) H. Conrad: Mater. Sci. Eng. A **287** (2000) 227–237.
10) K. N. Tu: J. Appl. Phys. **94** (2003) 5451–5473.
11) H. Mizubayashi, T. Okamoto, K. Koyama and M. Horiuchi: Acta Mater. **46** (1998) 1257–1264.
12) H. Mizubayashi, T. Usui and H. Tanimoto: J. Non-Crystalline Solids, **312–314** (2002) 542–546.
13) H. Mizubayashi, N. Kameyama, T. Hao and H. Tanimoto: Phys. Rev. B **64** (2001) 054201.
14) H. Mizubayashi, T. Hao and H. Tanimoto: J. Non-Crystalline Solids, **312–314** (2002) 581–584.
15) T. Hao, H. Tanimoto and H. Mizubayashi: Mater. Trans. JIM **46** (2005) 2898–2907.
16) *Binary Alloy Phase Diagrams 2nd ed.*, eds. T. B. Massalski, H. Okamoto, P. R. Subramanian, L. Kacprzak, (ASM International, 1990).
17) R. Takemoto: Thesis, Univ. Tsukuba 1995 (Japan).
18) R. L. Freed and J. B. Vander-Sandle: J. Non-cryst. Sol. **27** (1978) 9–28.
19) Z. Altounian, T. Guo-hua and J. O. Strom-Olsen: J. Appl. Phys. **53** (1982) 4755–4760.
20) N. S. Saxena: J. Non-cryst. Sol. **196** (1996) 37–44.
21) T. Takahashi, H. Tanimoto and H. Mizubayash: Mater. Sci. Eng. A **422** (2006) 297–301.
22) P. Yu, H. Y. Bai, M. B. Tang and W. L. Wang: J. Non-cryst. Sol. **351** (2005) 1328–1332.
23) Y. Yokoyama, K. Fukaura and A. Inoue: Mater. Sci. Eng. A **375–377** (2004) 427–431.
24) R. S. Qin, S. X. Su, J. D. Guo, G. H. He and B. L. Zhou: Nanostr. Mater. **10** (1998) 71–76.